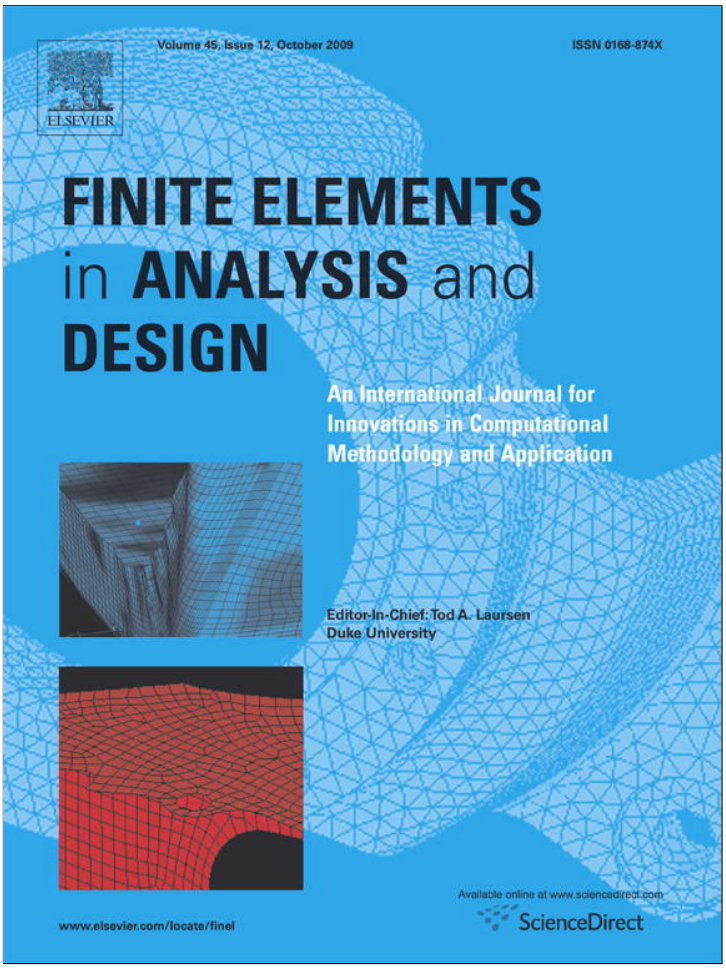

Finite Elements in Analysis and Design 45 (2009) 934–943

Contents lists available at ScienceDirect

Finite Elements in Analysis and Design

journal homepage: www.elsevier.de/locate/finel

Alternative stress-integration schemes for large-deformation problems of solid mechanics

Majidreza Nazem *, John P. Carter, Daichao Sheng, Scott W. Sloan

Centre for Geotechnical and Materials Modelling, School of Engineering, The University of Newcastle, NSW 2308, Australia

ARTICLE INFO

Article history:
Received 6 February 2009
Received in revised form
28 September 2009
Accepted 28 September 2009

Keywords:
Large deformation
Stress integration
Finite elements

ABSTRACT

In solving nonlinear problems of solid mechanics by the finite-element method, stresses at integration points are usually obtained by integrating nonlinear constitutive equations, given known incremental strains. In a large-deformation analysis, stress–strain relationships must be frame independent such that any rigid-body motion does not induce strain within the material. This principle is generally satisfied by introducing an objective stress rate, such as the Jaumann or Truesdell stress rates, into the constitutive equations. This paper investigates three alternative algorithms for integrating stress–strain relationships in a large-deformation analysis. It is shown that the effect of rigid-body motion is equivalent to a stress transformation and this transformation can be introduced before, after or during integration of the stress–strain constitutive equations. Although there is no theoretical advantage, in terms of accuracy, for selecting one of these strategies over the others, in terms of efficiency of algorithms one is more advantageous than the others. Performance of the proposed algorithms is studied and compared by means of numerical examples. The results of this study can be used in the development of fast and robust algorithms for stress integration of constitutive equations in nonlinear finite-element analysis.

1. Introduction

During an elastoplastic small-strain analysis by the finite-element method, loads are usually applied in increments and the corresponding incremental displacements are obtained by solving global equilibrium equations. The incremental strains can be computed from incremental displacements and these strains are then used to determine stresses within the continuum. For integration points that yield plastically the incremental stresses are then obtained by integrating constitutive equations. In a large-deformation analysis the stress–strain relations must be objective. Objectivity requires that the constitutive equations must be frame independent, i.e., rigid-body motions should not induce any strain in the material. This principle is generally satisfied by introducing an objective stress rate, such as the Jaumann or the Truesdell stress rate, into the stress–strain relations, e.g., [4,5]. A brief overview of how this has been achieved in practice is described below.

Hughes and Winget [9] introduced the concept of incremental objectivity of a stress-integration algorithm and presented an integration scheme for rate-type constitutive equations. The main achievement of this algorithm was providing a convenient framework for an objective transformation of the Cauchy stress tensor due to rigid-body rotations based on the Jaumann stress rate. Pinsky et al. [12] stated that a stress-integration algorithm for rate-type constitutive equations must satisfy three requirements: consistency, numerical stability, and incremental objectivity. Based on the Lie derivative of a spatial tensor, they developed an implicit stress-integration scheme with arbitrary objective stress rates satisfying the above conditions. The proposed scheme was then used to integrate constitutive equations of hyperelastic, hypoelastic, and elastoplastic materials.

Rodriguez-Ferran and Huerta [13] presented two stress update algorithms in large strain solid mechanics. The first algorithm, based on the work by Bathe et al. [2], used the Green–Lagrange strain tensor as the strain measure while the second algorithm incorporated the midstep configuration, where the symmetrised gradient of displacement increment was employed as the strain measure. They discussed implementation aspects and accuracy of the algorithms and found that the second algorithm is generally more accurate than the first. However, it would appear that efficiency of the algorithms was not studied by the authors. Later, Gadala and Wang [8] compared different integration algorithms for a rate-type constitutive equation based on the use of Jaumann stress rate as well as Truesdell stress rate. They used an implicit return mapping algorithm for integrating the constitutive equations and found that stress transformation due to rigid-body motion can be applied either before or after return mapping. Aspects of integrating constitutive equation involving large deformations, particularly in geotechnical problems, were presented by Nazem et al. [10]. In this paper, the authors discussed

* Corresponding author. Fax: +61 2 49216991.
E-mail address: majidreza.nazem@newcastle.edu.au (M. Nazem).

0168-874X/$ - see front matter © 2009 Elsevier B.V. All rights reserved.
doi:10.1016/j.finel.2009.09.006

problems with stress integration using a total-Lagrangian formulation and they studied the accuracy of different stress rates in an updated Lagrangian formulation.

Research on integration of constitutive equations in a large-deformation analysis is usually devoted to studying the accuracy of algorithms, mostly neglecting the question of their efficiency. However, the computational time spent integrating the constitutive equations in a nonlinear analysis is not negligible. Robust and efficient algorithms can, of course, reduce the cost of analysis significantly. In this paper, three alternative algorithms for integrating a rate-type constitutive equation are presented. These algorithms are based on the explicit integration scheme developed by Sloan [14]. Detailed implementation of these algorithms is discussed. Efficiency as well as accuracy of the algorithms are studied by solving the indentation of a rigid footing and a consolidation analysis of a rigid footing, both analyses requiring a large-deformation approach.

2. Stress integration

2.1. Small-strain problems

During a typical time step of a finite-element analysis, a set of ordinary differential equations must be solved to find the stress increment based on a known strain increment. This system of equations my be written in the following form:

$$\begin{aligned}\dot{\sigma}_{ij} &= C^{ep}_{ijkl}\dot{\varepsilon}_{kl}\\ \dot{\kappa}_i &= B_i(\sigma,\kappa)\dot{\lambda}\end{aligned} \tag{1}$$

where σ_{ij} is the true (Cauchy) stress tensor, ε_{ij} denotes the strain tensor, κ_i represents a set of hardening parameters, B is a function derived from the hardening laws, and

$$C^{ep}_{ijkl} = C^{e}_{ijkl} - \frac{C^{e}_{ijmn}(\partial f/\partial\sigma_{mn})C^{e}_{klpq}(\partial g/\partial\sigma_{pq})}{(\partial f/\partial\sigma_{pq})C^{e}_{pqrs}(\partial f/\partial\sigma_{rs}) - (\partial f/\partial\kappa_m)B_m(\sigma,\kappa)} \tag{2}$$

$$\dot{\lambda} = \frac{(\partial f/\partial\sigma_{ij})C^{e}_{ijkl}\dot{\varepsilon}_{kl}}{(\partial f/\partial\sigma_{ij})C^{e}_{ijkl}(\partial g/\partial\sigma_{kl}) - (\partial f/\partial\kappa_m)B_m(\sigma,\kappa)} = D_{kl}\dot{\varepsilon}_{kl} \tag{3}$$

in which C^e represents the elastic stress–strain matrix, f is a yield surface describing the elastic domain in stress space, g is the plastic potential function, and $\dot{\lambda}$ is a positive scalar called the plastic multiplier.

Eq. (1) is a system of ordinary differential equations, which needs to be integrated to determine the stress state. For a given strain increment, this integration takes the form

$$\begin{aligned}\sigma^{t+\Delta t}_{ij} &= \sigma^{t}_{ij} + \int_0^{\Delta\varepsilon_{kl}} C^{ep}_{ijkl}(\sigma,\kappa)d\varepsilon_{kl}\kappa^{t+\Delta t}_i = \kappa^{t}_i + \int_0^{\Delta\varepsilon_{kl}} B_i(\sigma,\kappa)d\lambda\\ &= \kappa^{t}_i + \int_0^{\Delta\varepsilon_{kl}} B_i(\sigma,\kappa)D_{kl}(\sigma,\kappa)d\varepsilon_{kl}\end{aligned} \tag{4}$$

in which D is a vector dependent on the current stresses and hardening parameters.

A stress-integration scheme is termed explicit if all stress dependent quantities such as the tensors C, B, and D are evaluated at known stress states. Otherwise, it is called an implicit scheme.

Crisfield [6] provides a comprehensive discussion of various stress-integration schemes. One of the most well-known implicit integration schemes is the backward Euler algorithm which employs an elastic predictor along with a plastic return mapping. This scheme normally requires second-order derivatives of the plastic potential as well as the yield function, making its implementation difficult for complex yield surfaces. Sloan [14] proposed an explicit algorithm with substepping and error control. This scheme, on the other hand, requires the intersection of stress path with the yield surface, which involves the solution of a nonlinear equation.

2.2. Large-deformation problems

For large-deformation analysis, stress–strain relations can no longer be expressed by Eq. (1) since components of true stresses change due to possible rigid-body motion. In other words, rigid-body rotation (or translation) must not change the strain in the material. This condition is usually satisfied by introducing an objective stress rate into the stress–strain relations. The choice of the objective stress rate is not unique and the most commonly used stress rates are the Jaumann stress rate ($\sigma^{\nabla J}$) and the Truesdell stress rate ($\sigma^{\nabla T}$), which are each defined as follows (e.g., see [3]):

$$\sigma^{\nabla J}_{ij} = \frac{d\sigma_{ij}}{dt} - \sigma_{ik}w_{jk} - w_{ik}\sigma_{kj} \tag{5}$$

$$\sigma^{\nabla T}_{ij} = \frac{d\sigma_{ij}}{dt} + \sigma_{ij}l_{kk} - \sigma_{ik}l_{jk} - l_{ik}\sigma_{kj} \tag{6}$$

in which w and l represent the spin tensor and the velocity gradient tensor, respectively, as follows:

$$w_{ij} = \frac{1}{2}\left(\frac{\partial v_i}{\partial x_j} - \frac{\partial v_j}{\partial x_i}\right) \tag{7}$$

$$l_{ij} = \frac{\partial v_i}{\partial x_j} \tag{8}$$

where v_i represents the velocity vector.

Introducing the Jaumann stress rate into small-strain constitutive equations, the stress increment is found by integrating $d\sigma$ in Eq. (5) along a given strain increment:

$$\begin{aligned}\sigma^{t+\Delta t}_{ij} &= \sigma^{t}_{ij} + \int_0^{\Delta\varepsilon_{ij}} d\sigma_{ij} = \sigma^{t}_{ij} + \int_0^{\Delta\omega_{kl}} (\sigma_{ik}\,d\omega_{jk} + \sigma_{jk}\,d\omega_{ik})\\ &\quad + \int_0^{\Delta\varepsilon_{kl}} C_{ijkl}(\sigma,\kappa)d\varepsilon_{kl}\end{aligned} \tag{9}$$

where

$$\omega_{ij} = \frac{1}{2}\left(\frac{\partial u_i}{\partial x_j} - \frac{\partial u_j}{\partial x_i}\right) \tag{10}$$

and u_i represents the displacement vector. Note that $C(\sigma,\kappa)$ in (9) refers to the constitutive matrix with respect to the configuration at time t and is a function of the current Cauchy stresses. To perform the integration in (9) a stress-integration scheme used for small deformation has to be modified to include the additional terms due to rigid-body motion. Considering the skew symmetry of $\Delta\omega_{ij}$, it is possible to show that the integration of rigid-body rotation in (9) is equivalent to a stress transformation [9]:

$$\sigma^{t}_{ij} + \int_0^{\Delta\omega_{kl}} (\sigma_{ik}\,d\omega_{kj} + \sigma_{jl}\,d\omega_{li}) = Q_{ik}\sigma^{t}_{kl}Q_{jl} \tag{11}$$

with

$$Q_{ij} = (\delta_{ik} - \beta\,\Delta\omega_{ik})^{-1}(\delta_{kj} + (1-\beta)\Delta\omega_{kj}) \tag{12}$$

where β is an integration parameter varying between 0 and 1. Therefore, the stress integration can be carried out as

$$\begin{aligned}\tilde{\sigma}^{t}_{ij} &= Q_{ik}\sigma^{t}_{kl}Q_{jl}\sigma^{t+\Delta t}_{ij} = \tilde{\sigma}^{t}_{ij} + \int_0^{\Delta\varepsilon_{kl}} C_{ijkl}(\tilde{\sigma},\kappa)d\varepsilon_{kl}\kappa^{t+\Delta t}_i\\ &= \kappa^{t}_i + \int_0^{\Delta\varepsilon_{kl}} B_i(\tilde{\sigma},\kappa)D_{kl}(\tilde{\sigma},\kappa)d\varepsilon_{kl}\end{aligned} \tag{13}$$

The integration in (13) is almost identical to the integration in (4) for small deformation. The only modification is that stresses at the

start of the increment should be transformed according to the first equation of (13). Therefore, standard integration schemes used for small deformation, either explicit or implicit, can be used with this formulation to update stresses and hardening parameters in (13).

Alternatively, one may integrate the stress–strain equation at the start of the increment and then transform stresses according to (11) as shown in the following:

$$\sigma_{ij}^{t+\Delta t} = \sigma_{ij}^{t} + \int_0^{\Delta\varepsilon_{kl}} C_{ijkl}(\sigma,\kappa)\,d\varepsilon_{kl}\,\kappa_i^{t+\Delta t} = \kappa_i^{t} + \int_0^{\Delta\varepsilon_{kl}} B_i(\sigma,\kappa)\cdot D_{kl}(\sigma,\kappa)\,d\varepsilon_{kl}\,\tilde{\sigma}_{ij}^{t+\Delta t} = Q_{ik}\sigma_{kl}^{t+\Delta t}Q_{jl} \tag{14}$$

It is also possible to include rigid-body rotations by introducing the Truesdell stress rate into the constitutive equations. Gadala and Wang [8] showed that the following stress transformation and stress integration is equivalent to the Truesdell stress rate defined by (6):

$$\sigma_{ij}^{t+\Delta t} = \sigma_{ij}^{t} + \int_0^{\Delta\varepsilon_{ij}} d\sigma_{ij} = \frac{1}{J}\,{}^{t}F_{ik}^{t+\Delta t}(\sigma_{kl}^{t})\,{}^{t}F_{jl}^{t+\Delta t} + \int_0^{\Delta\varepsilon_{kl}} C_{ijkl}(\sigma,\kappa)\,d\varepsilon_{kl} \tag{15}$$

where F denotes the deformation gradient defined by

$${}^{t}F_{ij}^{t+\Delta t} = \frac{\partial x_i^{t+\Delta t}}{\partial x_j^{t}} \tag{16}$$

and J is its determinant; x represents the spatial configuration of a material point. The right superscript denotes the time when the quantities are measured. Note that in an updated Lagrangian formulation all quantities are measured with respect to the last equilibrium configuration (i.e., at time t).

3. Alternative integration schemes

Eqs. (9) and (15) show that the effect of rigid-body motion must be introduced to the constitutive equations during stress integration. This effect can be introduced before, after, or during integration of the constitutive equations, which provides three alternative approaches. However, no obvious theoretical advantage exists for selecting one of these strategies. Moreover, it would appear that advantages and disadvantages of one strategy over the two others have not yet been reported in the literature (e.g., see [8]). This study attempts to compare alternative schemes for integrating the stress–strain relations in a large-deformation analysis. In the following, these algorithms are explained in more detail.

3.1. Algorithms based on schemes for small-displacement analysis

As mentioned before, effects of rigid-body motion can be introduced either before or after integration of the constitutive equations. For the formulation using the Jaumann stress rate, such an approach results in two alternative stress-integration schemes as shown by Eqs. (13) and (14). The main advantage of this approach is that the numerical schemes used to integrate the constitutive equations for small displacement can also be used for large-deformation analysis. To explain this approach in more detail, we first present the following algorithms for correcting the stresses due to rigid-body motion. Algorithm (a) applies to the formulation using the Jaumann stress rate, while Algorithm (b) applies to the formulation using the Truesdell stress rate.

Algorithm (a). Stress transformation for rigid-body motion (Jaumann stress rate):

(1) Enter with stresses ${\sigma_{ij}}^{t}$ and the spin tensor increment $\Delta\omega_{ij}$.
(2) Calculate Q_{ij} by

$$Q_{ij} = \left(\delta_{ik} - \frac{1}{2}\Delta\omega_{ik}\right)^{-1}\left(\delta_{kj} + \frac{1}{2}\Delta\omega_{kj}\right).$$

(3) Find $\tilde{\sigma}_{ij}^{t}$ by $\tilde{\sigma}_{ij}^{t} = Q_{ik}\sigma_{kl}^{t}Q_{jl}$.
(4) Exit with corrected stresses $\tilde{\sigma}_{ij}^{t}$.

Note that to ensure objectivity the spin tensor increment is evaluated with respect to the configuration at the midpoint of a load increment, i.e., β=0.5 in Eq. (12).

Algorithm (b). Stress transformation for rigid-body motion (Truesdell stress rate):

(1) Enter with stresses ${\sigma_{ij}}^{t}$, the deformation gradient ${}^{t}F_{ij}^{t+\Delta t}$, and its determinant J.
(2) Compute $\overline{\sigma}_{ij}^{t}$ by

$$\overline{\sigma}_{ij}^{t} = \frac{1}{J}\,{}^{t}F_{ik}^{t+\Delta t}(\sigma_{kl}^{t})\,{}^{t}F_{jl}^{t+\Delta t}.$$

(3) Exit with corrected stresses $\overline{\sigma}_{ij}^{t}$.

The algorithms above can be applied either at the start of the increment, leading to Algorithm 1, or applied at the end of the increment, leading to Algorithm 2.

Algorithms 1(a) and (b). Transformation followed by integration:

(1) Enter with stresses ${\sigma_{ij}}^{t}$, the strain increment $\Delta\varepsilon_{ij}$, and the spin tensor increment $\Delta\omega_{ij}$.
(2) Call Algorithm (a) or (b) with ${\sigma_{ij}}^{t}$ and $\Delta\omega_{ij}$ to find $\tilde{\sigma}_{ij}^{t}$.
(3) Call the stress-integration scheme with $\overline{\sigma}_{ij}^{t}$ and $\Delta\varepsilon_{ij}$ to find ${\sigma_{ij}}^{t+\Delta t}$.
(4) Exit with final stresses ${\sigma_{ij}}^{t+\Delta t}$.

Algorithms 2(a) and (b). Integration followed by transformation:

(5) Enter with stresses ${\sigma_{ij}}^{t}$, the strain increment $\Delta\varepsilon_{ij}$, and the spin tensor increment $\Delta\omega_{ij}$.
(6) Call the stress-integration scheme with ${\sigma_{ij}}^{t}$ and $\Delta\varepsilon_{ij}$ to find ${\sigma_{ij}}^{t+\Delta t}$.
(7) Call Algorithm (a) or (b) with ${\sigma_{ij}}^{t+\Delta t}$ and $\Delta\omega_{ij}$ to find $\tilde{\sigma}_{ij}^{t+\Delta t}$.
(8) Exit with final stresses $\tilde{\sigma}_{ij}^{t+\Delta t}$.

Algorithms 1(a), (b) and 2(a), (b) provide two simple procedures to integrate the stress–strain relations in a large-deformation analysis. Both algorithms preserve the principle of stress objectivity and they require only an auxiliary subroutine to correct the stresses due to possible rigid-body motion. For some cases the stress-integration schemes used in small-displacement analysis, such as that introduced by Sloan et al. [15,16], can then be used directly in large-deformation analysis.

The basic assumption in Algorithms 1(a), (b) and 2(a), (b) is that straining and rigid-body motions can be applied sequentially over the increment, even though the two increments are derived from the same displacement increment and hence should occur simultaneously. An obvious improvement would be to apply the strain increment and the rigid-body rotation increment simultaneously during stress integration.

3.2. Algorithms for proportional straining and rotation

Since straining and rigid-body motions are derived from the same displacement increment, it is also reasonable to assume that the two quantities can be integrated proportionally over the

increment. For example, if we subdivide the strain increment into two subincrements during stress integration, we should also subdivide the rigid-body rotation increment into two subincrements proportionally.

Sloan [14] developed an explicit scheme for integration of constitutive equations in the form of (4) for small-displacement analysis. This scheme was originally designed for conventional elastoplastic models, which are characterised by linearly elastic and perfect plastic behaviour. Subsequently, Sloan et al. [15,16] introduced a number of enhancements to the original scheme. In their latter work, the scheme was extended to cover generalised critical state-type models (originally developed for soil), which exhibit nonlinear elastic behaviour inside the yield surface. This stress-integration scheme controls the error in computed stresses by using a local error measure to automatically subincrement the applied strain increment. The error measure is computed at each integration point by taking the difference between a first-order accurate Euler solution and a second-order accurate modified Euler solution. This method has been used to solve problems involving a wide range of complicated constitutive models for soils [15,17]. In this section of the paper, the algorithms developed by Sloan et al. [15,16] are generalised for large-deformation elastoplastic analysis and a general stress-integration scheme is presented for large-deformation problems.

3.2.1. Problem definition

The proportional problem is first formulated using the Jaumann stress rate. This formulation can be easily extended to the Truesdell stress rate. Based on the Jaumann stress rate in (5) and (9), the system of ordinary differential equations to be solved during a stress-integration procedure in a large-deformation analysis are expressed in the following form:

$$\dot{\sigma}_{ij} = C^{ep}_{ijkl}\dot{\varepsilon}_{kl} + \sigma^t_{ik}\dot{\omega}_{kj} + \sigma^t_{jl}\dot{\omega}_{il} \tag{17}$$

$$\dot{\kappa}_i = B_i(\sigma,\kappa)\dot{\lambda} \tag{18}$$

To integrate Eqs. (17) and (18) numerically, a pseudo-time T is introduced by

$$T = \frac{t - t_0}{\Delta t} \tag{19}$$

where t_0 is the time at the start of the strain increment and $t_0+\Delta t$ is the time at the end of the increment. Applying the chain rule of differentiation to Eqs. (17) and (18) gives

$$\begin{aligned}\frac{d\sigma_{ij}}{dT} &= C^{ep}_{ijkl}\Delta\varepsilon_{kl} + \sigma^t_{ik}\,\Delta\omega_{kj} + \sigma^t_{jl}\,\Delta\omega_{il} \\ &= \Delta\sigma^e_{ij} - \Delta\lambda\, C^e_{ijkl}\cdot\frac{\partial g}{\partial\sigma_{kl}} + \sigma^t_{ik}\,\Delta\omega_{kj} + \sigma^t_{jl}\,\Delta\omega_{il}\end{aligned} \tag{20}$$

$$\frac{d\kappa_i}{dT} = B_i(\sigma,\kappa)\Delta\lambda \tag{21}$$

where

$$\begin{aligned}\Delta\lambda &= \frac{(\partial f/\partial\sigma_{ij})C^e_{ijkl}\,\Delta\varepsilon_{kl}}{(\partial f/\partial\sigma_{ij})C^e_{ijkl}(\partial g/\partial\sigma_{kl}) - (\partial f/\partial\kappa_m)B_m(\sigma,\kappa)} \\ &= \frac{(\partial f/\partial\sigma_{ij})\Delta\sigma^e_{ij}}{(\partial f/\partial\sigma_{ij})C^e_{ijkl}(\partial g/\partial\sigma_{kl}) - (\partial f/\partial\kappa_m)B_m(\sigma,\kappa)}\end{aligned} \tag{22}$$

Eqs. (20) and (21) define an initial-value problem to be integrated over the pseudo-time interval $T=0$ to $T=1$.

3.2.2. Intersection with the yield surface

If the initial-stress state is inside the yield surface and the strain increment causes plastic yielding, the strain increment can be decomposed into a purely elastic part and an elastoplastic part. The elastic part of the strain increment produces a stress increment that moves the stress point, previously inside the yield surface, to the yield surface. The rigid-body correction should thus be applied also in two stages. The spin tensor increment in the first stage is consistent with the elastic strain increment, while the second correction is commensurate with the elastoplastic strain increment.

To start the stress integration, it is assumed that the whole strain increment is elastic. The rigid-body rotation effect, $\Delta\tilde{\sigma}_{ij}$, is found by considering the total spin tensor increment, using Algorithm (a). The trial elastic-stress increments $\Delta\sigma_{ij}{}^e$ and $\Delta\tilde{\sigma}_{ij}$ are then used to check if the stress state has changed from elastic to plastic. Such a change occurs if $f(\sigma^t_{ij},\kappa^t_i)<0$ but $f(\sigma^t_{ij}+\Delta\sigma^e_{ij}+\Delta\tilde{\sigma}_{ij},\kappa^t_i)>0$. If such a stress change occurs, it is necessary to ascertain the fractions of $\Delta\varepsilon_{ij}$ and $\Delta\omega_{ij}$, α, that move the stresses from σ^t_{ij} to the stress state σ^t_{int} on the yield surface, as shown in Fig. 1. Note that σ^t_{int} includes the correction of stresses due to rigid-body rotation according to the proportional spin tensor increment $\alpha\,\Delta\omega_{ij}$, denoted by $\Delta\tilde{\sigma}^{\alpha}_{ij}$. This correction may be obtained by Algorithm (a) or (b) with initial values for the stress and the spin tensor increment being σ^t_{ij} and $\alpha\,\Delta\omega_{ij}$, respectively. Also note that, in Fig. 1, the exact yield condition $f(\sigma_{ij},\kappa_i)=0$ is replaced by the approximation $|f(\sigma_{ij},\kappa_i)\le FTOL|$ to allow for the effects of finite-precision arithmetic, where $FTOL$ is a small positive tolerance and is usually in the range 10^{-6}–10^{-9}. The problem of finding stresses at the yield surface intersection point σ^t_{int} is equivalent to finding the scalar quantity α that satisfies the nonlinear equation

$$f(\sigma^t_{ij} + \alpha\overline{C}^e_{ijkl}\,\Delta\varepsilon_{kl} + \Delta\tilde{\sigma}^{\alpha}_{ij},\kappa^t_i) = f((\sigma^t_{ij})_{int},\kappa^t_i) = 0 \tag{23}$$

Note that in (23) the secant elastic constitutive matrix $\bar{C}^e$ is used, which for linear elasticity is identical to the tangential elastic constitutive matrix. For critical state soil models, the elastic response is obtained by

$$\Delta\overline{\sigma}^e_{ij} = \overline{C}^e_{ijkl}(\overline{K},\overline{G})\Delta\varepsilon_{kl} = \overline{C}^e_{ijkl}(\sigma^t,\Delta\varepsilon_v)\Delta\varepsilon_{kl} \tag{24}$$

where $\bar{K}$ and $\bar{G}$ are the secant elastic moduli evaluated using the initial stress and the total volumetric strain $\Delta\varepsilon_v$ increment. The nonlinear equation in (23) can be solved by an iterative procedure such as Pegasus, which was suggested by Dowell and Jarratt [7]. For more details see Sloan et al. [15].

3.2.3. Elastoplastic unloading

An elastic–plastic transition may occur if a previously yielded stress point is subjected to an elastoplastic stress increment of the type shown in Fig. 2. This type of stress path can occur near the tip of a failure surface if $\Delta\overline{\sigma}^e_{ij}$ is large owing to the use of discrete load increments, and does not require unloading of the overall structure. Since the portion of the stress path inside the yield surface is elastic, the elastoplastic constitutive law needs to be

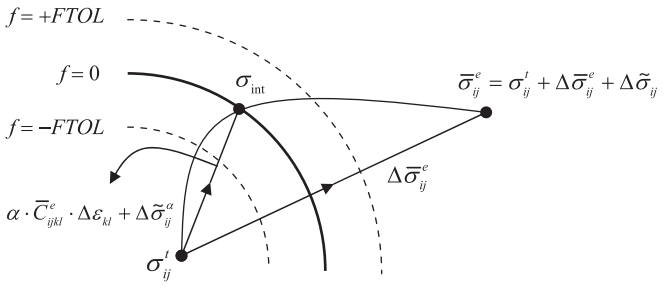

Fig. 1. Yield surface intersection: transition from elastic to plastic state.

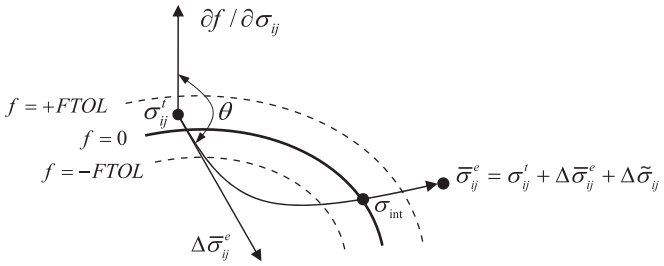

Fig. 2. Yield surface intersection: elastoplastic unloading.

integrated only beyond the last intersection point. The situation arises when the angle θ between the yield surface gradient $a_{ij}{}^t=\partial f/\partial\sigma_{ij}{}^t$ and the tangential elastic stress increment $\Delta\sigma_{ij}{}^e$ is larger than 90° and $f(\sigma_{ij}^e,\kappa_i^t)>+FTOL$. The first condition may be written as

$$\cos\theta=\frac{a_{ij}^t\,\Delta\sigma_{ij}^e}{\|a_{ij}^t\|_2\|\Delta\sigma_{ij}^e\|_2}<-LTOL \tag{25}$$

in which *LTOL* is a suitable tolerance. The procedure for finding the yield surface intersection for elastoplastic unloading is similar to the algorithm used to find the intersection with the yield surface. To ensure the algorithm finds the correct crossing, it is sufficient to determine starting values, α_0 and α_1, which satisfy $f(\sigma_{ij}^t+\alpha_0\overline{C}_{ijkl}^e\,\Delta\varepsilon_{ij},\kappa_i^t)<-FTOL$ and $f(\sigma_{ij}^t+\alpha_1\overline{C}_{ijkl}^e\,\Delta\varepsilon_{ij},\kappa_i^t)>FTOL$.

3.2.4. Modified Euler method for stress integration

In the following, the main algorithm to solve the system of differential equations defined by (20) and (21) will be presented. This algorithm is based on the approach first published by Sloan [14], which attempts to control the errors in stresses and hardening parameter by using a local error measure to automatically subincrement the imposed strain increment. For each subincrement, the local error measure is found by taking the difference between a second-order-accurate modified Euler solution and a first-order-accurate Euler solution. Once the local error has been computed for a given step, the size of the next step is determined using an expression for the dominant error term. This type of error control permits the size of each subincrement to vary throughout the integration process, depending on the nonlinearity of the constitutive relations. Consider a pseudo-time subincrement in the range $0<\Delta T^n\le 1$ and let the subscripts n and $n+1$ denote quantities evaluated at the pseudo-times T^n and $T^{n+1}=T^n+\Delta T^n$. With the explicit Euler method, the values for σ_{ij} and κ_i at the end of a pseudo-time step ΔT^n are found from

$$\sigma_{ij}^{n+1}=\sigma_{ij}^n+\Delta\sigma_{ij}^1\kappa_i^{n+1}=\kappa_i^n+\Delta\kappa_i^1 \tag{26}$$

where

$$\Delta\sigma_{ij}^1=C_{ijkl}^{ep}(\sigma^n,\kappa^n)\Delta\varepsilon_{kl}^n\Delta\kappa_i^1=\Delta\lambda(\sigma^n,\kappa^n,\Delta\varepsilon^n)B_i(\sigma^n) \tag{27}$$

and

$$\Delta\varepsilon_{ij}^n=\Delta T^n\,\Delta\varepsilon_{ij} \tag{28}$$

A more accurate estimate of the stresses and hardening parameter at the end of the interval ΔT^n can be found using the modified Euler procedure. This gives

$$\tilde{\sigma}_{ij}^{n+1}=\sigma_{ij}^n+\frac{1}{2}(\Delta\sigma_{ij}^1+\Delta\sigma_{ij}^2)+\Delta\tilde{\sigma}_{ij}^{1-\alpha}\quad\tilde{\kappa}_i^{n+1}=\kappa_i^n+\frac{1}{2}(\Delta\kappa_i^1+\Delta\kappa_i^2) \tag{29}$$

where $\Delta\sigma_{ij}{}^1$ and $\Delta\kappa_i{}^1$ are computed from the Euler scheme, $\Delta\tilde{\sigma}_{ij}^{1-\alpha}$ represents a correction to stress tensor due to $(1-\alpha)\Delta\omega_{ij}$, and

$$\begin{aligned}\Delta\sigma_{ij}^2&=C_{ijkl}^{ep}(\sigma^n+\Delta\sigma^1,\kappa^n+\Delta\kappa^1)\Delta\varepsilon_{kl}^n\Delta\kappa_i^2\\&=\Delta\lambda(\sigma^n+\Delta\sigma^1,\kappa^n+\Delta\kappa^1,\Delta\varepsilon^n)B_i(\sigma^n+\Delta\sigma^1)\end{aligned} \tag{30}$$

The relative error measure is computed by

$$R^{n+1}=\frac{1}{2}\max\left\{\frac{\|\Delta\sigma_{ij}^2-\Delta\sigma_{ij}^1\|}{\|\tilde{\sigma}_{ij}^{n+1}\|},\quad\frac{\|\Delta\kappa_i^2-\Delta\kappa_i^1\|}{\|\tilde{\kappa}_i^{n+1}\|}\right\} \tag{31}$$

where the stresses are treated separately from the hardening parameters to allow for differences of scale. Once this error measure has been computed, the current strain subincrement is accepted if R^{n+1} is not greater than some prescribed tolerance, *STOL*, and rejected otherwise. Regardless of whether the subincrement is accepted or rejected, the next pseudo-time step is found by scaling the size of the current subincrement:

$$\Delta T^{n+1}=q\,\Delta T^n \tag{32}$$

where q is set to [15]

$$q=0.9\sqrt{\frac{STOL}{R^{n+1}}} \tag{33}$$

To avoid dramatic changes in step sizes, q is also limited by

$$0.1\le q\le 1.1 \tag{34}$$

so that

$$0.1\Delta T^{n-1}\le\Delta T^n\le 1.1\Delta T^{n-1} \tag{35}$$

The end of the integration procedure is reached when the entire increment of strain is applied so that

$$\sum\Delta T=T=1 \tag{36}$$

The complete explicit modified Euler algorithm with substepping for materials including hardening parameters may be summarised as follows.

Algorithm 3. Explicit modified Euler algorithm for elastoplastic models with hardening:

(1) Enter with initial stresses σ_{ij}^t, initial hardening parameters κ_i^t, the strain increment for the current load step $\Delta\varepsilon_{ij}$, the spin tensor increment $\Delta\omega_{ij}$, and the error tolerance for the stresses *STOL*.
(2) Find $\Delta\tilde{\sigma}_{ij}$ by Algorithm (a) and compute the stress increment $\Delta\sigma_{ij}^e$ and the trial elastic stress σ_{ij}^e according to
$\Delta\overline{\sigma}_{ij}^e=\overline{C}_{ijkl}^e\,\Delta\varepsilon_{kl}\overline{\sigma}_{ij}^e=\sigma_{ij}^t+\Delta\overline{\sigma}_{ij}^e+\Delta\tilde{\sigma}_{ij}$
If $f(\overline{\sigma}_{ij}^e,\kappa_i^t)\le FTOL$ then the stress increment is purely elastic, so set $\sigma_{ij}^{t+\Delta t}=\overline{\sigma}_{ij}^e$ and $\kappa_t{}^{t+\Delta t}=\kappa_i{}^t$ and go to step 14.
(3) If $f(\sigma_{ij}{}^t+\kappa_i{}^t)<-FTOL$ and $f(\overline{\sigma}_{ij}^e,\kappa_i^t)>FTOL$ then the stress point undergoes a transition from elastic to plastic behaviour. Compute the portion of strain increment that correspond to purely elastic deformation, α, and go to step 5.
(4) If $f(\sigma_{ij}{}^t+\kappa_i{}^t)\le FTOL$ and $f(\overline{\sigma}_{ij}^e,\kappa_i^t)>FTOL$, check for an elastoplastic unloading by computing
$\cos\theta=\dfrac{a_{ij}^t\,\Delta\sigma_{ij}^e}{\|a_{ij}^t\|_2\|\Delta\sigma_{ij}^e\|_2}$
If $\cos\theta\ge-LTOL$ then
Set $\alpha=0$
else
Compute the portion of $\Delta\varepsilon_{ij}$ and $\Delta\omega_{ij}$ that corresponds to purely elastic deformation α
else
The stress state is illegal as it lies outside the yield surface.
(5) Update the stresses at the onset of plastic yielding as $\sigma_{ij}^t\leftarrow\sigma_{ij}^t+\alpha\overline{C}_{ijkl}^e(\sigma^t,\alpha\,\Delta\varepsilon^v)\Delta\varepsilon_{kl}+\Delta\tilde{\sigma}_{ij}^{\alpha}$. Then compute the portion of $\Delta\sigma_{ij}^e$ that corresponds to plastic deformation according to $\Delta\sigma_{ij}{}^e\leftarrow(1-\alpha)\Delta\sigma_{ij}{}^e$ and update the spin tensor by $\Delta\omega_{ij}\leftarrow(1-\alpha)\Delta\omega_{ij}$.

(6) Set $T=0$ and $\Delta T=1$.
(7) While $T<1$, perform steps 8–14.
(8) Compute $\Delta\tilde{\sigma}_{ij}^{I}$ and $\Delta\kappa_i^I$ for $I=1$–2 using

$$\Delta\tilde{\sigma}_{ij}^{I}=\Delta T\,\Delta\sigma_{ij}^{e}-\Delta\lambda^{I}C_{ijkl}^{e}\frac{\partial g}{\partial\tilde{\sigma}_{kl}^{I}}$$

$$\Delta\kappa_i^I=\Delta\lambda^{I}B_i(\tilde{\sigma}^{I},\tilde{\kappa}^{I})$$

where

$$\Delta\lambda^{I}=\max\left\{\frac{\Delta T\,C_{ijkl}^{e}(\partial f/\partial\tilde{\sigma}_{kl}^{I})}{(\partial f/\partial\tilde{\sigma}_{ij}^{I})C_{ijkl}^{e}(\partial g/\partial\tilde{\sigma}_{kl}^{I})-(\partial f/\partial\tilde{\kappa}_{m}^{I})B_m(\tilde{\sigma}^{I},\tilde{\kappa}^{t})},0\right\}$$

$$\tilde{\sigma}_{ij}^{1}=\sigma_{ij}^{T}$$

$$\tilde{\sigma}_{ij}^{2}=\sigma_{ij}^{T}+\Delta\sigma_{ij}^{1}$$

$$\tilde{\kappa}_i^{1}=\kappa_i^{T}$$

$$\tilde{\kappa}_i^{2}=\kappa_i^{T}+\Delta\kappa_i^{1}$$

Find $\Delta\tilde{\sigma}_{ij}$ by Algorithm (a) with initial stress tensor σ_{ij}^{T} and spin tensor $\Delta T\Delta\omega_{ij}$. Then compute the new stresses and hardening parameters and hold them in temporary storage according to

$$\tilde{\sigma}_{ij}^{T+\Delta T}=\sigma_{ij}^{T}+\frac{1}{2}(\Delta\sigma_{ij}^{1}+\Delta\sigma_{ij}^{2})+\Delta\tilde{\sigma}_{ij}$$

$$\tilde{\kappa}_i^{T+\Delta T}=\kappa_i^{T}+\frac{1}{2}(\Delta\kappa_i^{1}+\Delta\kappa_i^{2}).$$

(9) Determine the relative error for the current substep from

$$R_e^{T+\Delta T}=\max\left\{\frac{\|\Delta\sigma_{ij}^{2}-\Delta\sigma_{ij}^{1}\|}{2\|\tilde{\sigma}_{ij}^{T+\Delta T}\|},\frac{|\Delta\kappa_i^{2}-\Delta\kappa_i^{1}|}{2|\kappa_i^{T+\Delta T}|},EPS\right\}$$

where *EPS* is a machine constant indicating the smallest relative error that can be calculated.
(10) If $R_e^{T+\Delta T}>STOL$ the substep has failed. First compute

$$q=\max\left\{0.9\sqrt{\frac{STOL}{R_e^{T+\Delta T}}},0.1\right\}$$

and then set $\Delta T\leftarrow\max\{q\,\Delta T,\Delta T_{min}\}$ before returning to step 8.
(11) The substep is successful, so update the stresses and the hardening parameters by

$$\sigma_{ij}^{T+\Delta T}=\tilde{\sigma}_{ij}^{T+\Delta T}$$

$$\kappa_i^{T+\Delta T}=\tilde{\kappa}_i^{T+\Delta T}.$$

(12) Extrapolate to obtain the size of the next substep by computing

$$q=\min\left\{0.9\sqrt{\frac{STOL}{R_e^{T+\Delta T}}},1.1\right\}.$$

If the previous step failed, limit the step size growth further by enforcing:

$$q=\min\{q,1.0\}$$

Compute new step size and update pseudo-time according to

$$\Delta T\leftarrow q\,\Delta T,\qquad \Delta T\leftarrow T+\Delta T.$$

(13) Ensure the next step size is not smaller than the minimum step size and check that integration does not proceed beyond $T=1$ by setting

$$\Delta T\leftarrow\max\{\Delta T,\Delta T_{\min}\}$$

and then

$$\Delta T\leftarrow\min\{\Delta T,1-T\}.$$

(14) Exit with stresses σ_{ij}^{1} and hardening parameters κ_i^{1} at the end of the increment.

For double precision arithmetic, appropriate values for the tolerances in steps 4 and 10 are $LTOL\approx10^{-6}$ and $EPS\approx10^{-16}$.

In Algorithm 3, rigid-body corrections are introduced in both elastic and elastoplastic stress increments. One may notice that the total stress correction due to rigid-body rotation may be included in the elastic part only. However, the difference between such a scheme and Algorithm 1 is not of much significance in practice.

As a summary, three alternative algorithms for considering the principle of objectivity in a stress-integration scheme were explained in this section. This principle, which corresponds to the invariability of the stress state under rigid-body motion, was satisfied by using the Jaumann stress rate whilst other stress rates such as that of Truesdell may also be used. The performance of these algorithms will be studied and compared by means of numerical examples in the following.

4. Numerical examples

Three alternative algorithms for integrating the constitutive equations in a rate-type large-deformation analysis were presented in the previous section. The stress-integration procedures are explained in Algorithms 1(a), (b) and 2(a), (b) and 3. In Algorithm 1, the stress correction due to rigid-body rotations is applied before integrating the constitutive equations. Algorithm 2 integrates the stress–strain relation and then corrects the stresses for possible rigid-body motion. In Algorithm 3, the effect of rigid-body rotation is introduced both in elastic and the elastoplastic stress increments during the integration. These algorithms have been implemented in the finite-element code SNAC, developed at the University of Newcastle in Australia over the last two decades.

4.1. Rigid footing on undrained soil

In the first example, the plane-strain problem of a rough rigid footing on an undrained soil layer represented by an associated Tresca model is considered. A large footing displacement (deformation) is applied in order to study the accuracy and performance of Algorithms 1(a), (b) and 2(a), (b) and 3. The mesh for the right-hand half of the footing and material properties are

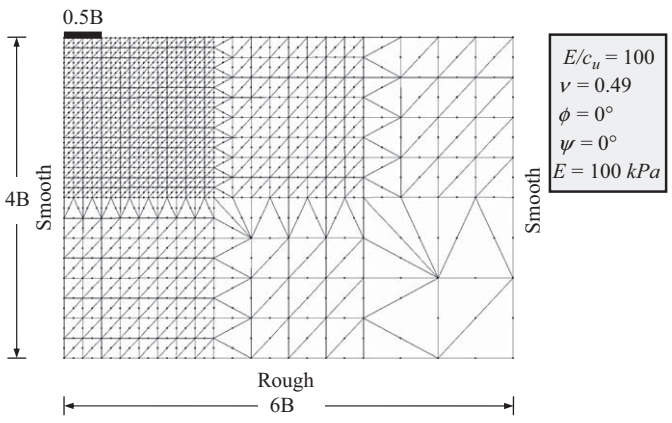

Fig. 3. Rigid rough footing on cohesive soil.

shown in Fig. 3. Note that c_u in Fig. 3 represents the undrained shear strength of the soil. Young's modulus has been deliberately assigned a small value of 100 kPa, which would probably be unrealistic for most soils, in order to include large elastic as well as large plastic deformations, and therefore to provide a rigorous test of the algorithms for both elasticity and elastoplasticity. The mesh used in these analyses consisted of 872 6-noded plane-strain isoparametric triangular elements, with six integration points per element. The total imposed displacement was equal to the footing width, B, and this was applied using 200 time increments. To study the performance of these algorithms under identical circumstances, the standard Newton–Raphson method is used to solve the nonlinear global equilibrium equations in this example.

The load–displacement curve obtained by the arbitrary Lagrangian–Eulerian (ALE) method based on the Jaumann stress rate was presented by Nazem et al. [10] and is shown here in Fig. 4. A comparison between the performance of the Jaumann stress rate and the Truesdell stress rate and the small-strain solution can be found in the same reference. It seems that at a footing displacement approaching the footing width the prediction of the ALE method approaches the exact collapse load for a rigid strip footing loaded at the bottom of a deep trench, i.e., $(2+2\pi)c_u \approx 8.28c_u$ (see [10] for more details and discussion). The deformed mesh at the end of analysis is shown in Fig. 5 for both symmetric halves of the footing. This undistorted mesh clearly shows that some elements around the footing experience relatively large rotations (in the order of 90°).

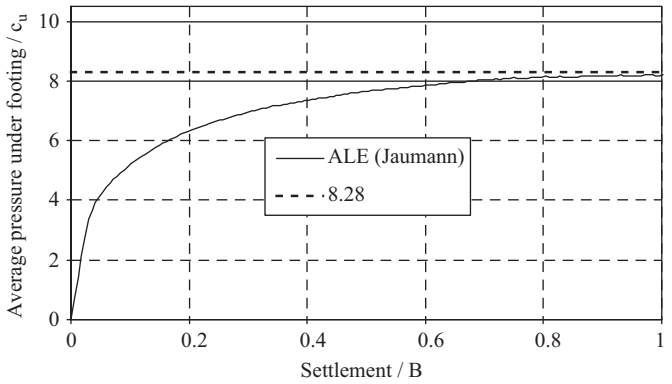

Fig. 4. Load–displacement response of the rigid rough footing on undrained soil.

This same example has been used here to investigate the performance of the alternative stress-integration algorithms described in previous sections. The footing problem was analysed by the ALE method based on the Jaumann stress rate using each algorithm individually. Load–displacement curves obtained by all algorithms are more or less the same as the plot shown in Fig. 4. This means that in terms of accuracy, all algorithms provide essentially the same solution provided that a small enough time step is used in the analyses. The size of time step may affect the accuracy of algorithms and this subject requires further investigation. To study the efficiency of each algorithm, the stress-integration time and the total number of iterations necessary to achieve equilibrium in each analysis are shown in Table 1. In terms of performance, the difference between Algorithms 1(a), (b) and 2(a), (b) is not significant. However, Algorithm 3 is 12% faster than Algorithm 1 and 11.6% faster than Algorithm 2.

The accuracy and performance of these algorithms in an updated Lagrangian (UL) analysis are also worth comparing, where the effect of large deformation is also taken into account but where significant mesh distortion is a possibility. To achieve this purpose, the problem was solved again using the same geometry and material properties but different Young's modulus. E was assumed to be 1000 kPa and a total displacement of $0.4B$ was applied to the footing using 200 time increments. Load–displacement curves obtained by all algorithms are identical but for brevity they are not shown here. The close agreement of these solutions is further evidence that accuracies of the algorithms are similar. However, in terms of efficiency Algorithm 3 outperforms Algorithms 1(a), (b) and 2(a), (b), as shown in Table 2. Note that

Table 1
Stress-integration time and total iterations of alternative stress-integration algorithms—ALE method.

Algorithm	Stress-integration time (s)	Total iterations
1	83	1236
2	86	1240
3	73	1219

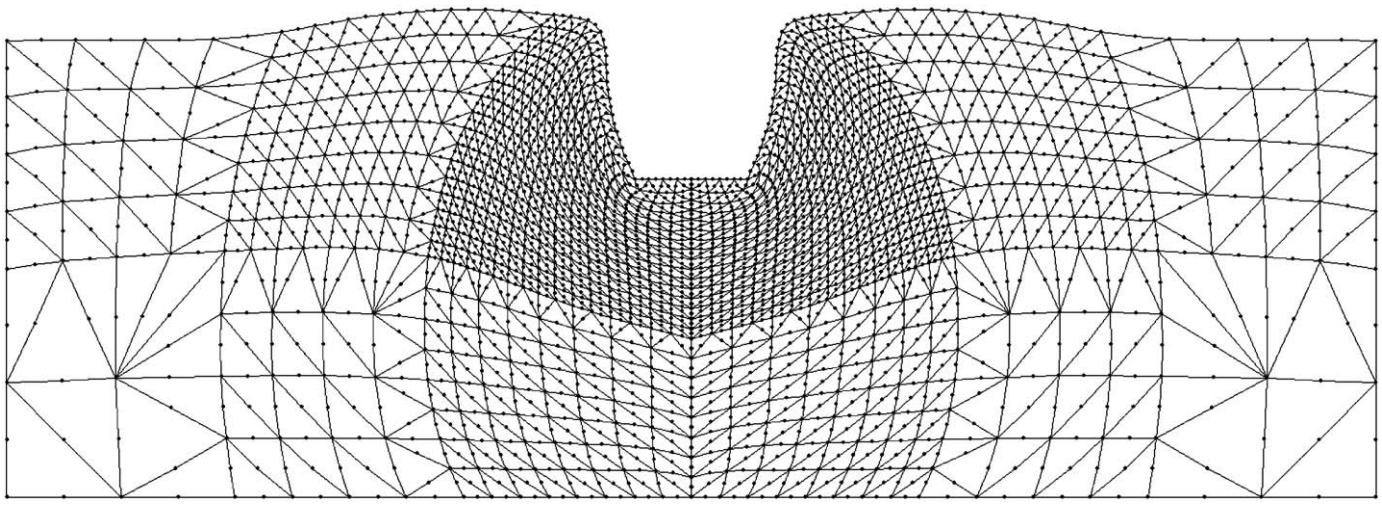

Fig. 5. Deformed mesh for footing on undrained soil—ALE method.

Table 2
Stress-integration time and total iterations of alternative stress-integration algorithms—UL method.

Algorithm	Stress-integration time (s)	Total iterations
1	27	635
2	31	769
3	22	602

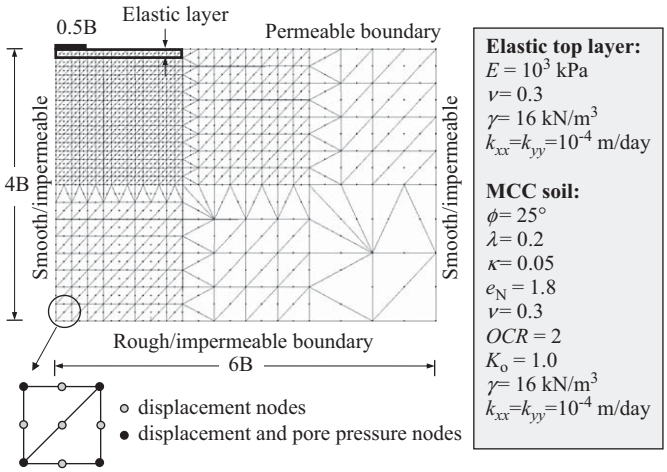

Fig. 6. Consolidation of rigid strip footing on MCC soil.

for this problem, Algorithm 3 is 18.5% faster than Algorithm 1 and 29% faster than Algorithm 2.

Finally, it is noted that this example involves significant rigid-body rotation, particularly of elements of soil below the edge of the footing, and so it provides a rigorous test of the various stress-integration algorithms.

4.2. Consolidation analysis of a footing on a modified cam-clay material

In this example, we study the performance of the suggested algorithms by solving the consolidation of a rigid strip footing on a modified Cam-Clay material (MCC), a more complex soil model, which can simulate strain softening and hardening via one hardening parameter (the preconsolidation pressure). The formulation and details of the coupled analysis performed here were previously presented by Nazem et al. [11]. The geometry, finite-element mesh, and material properties are shown in Fig. 6. The parameters in Fig. 6 include

- φ the friction angle of the soil skeleton
- λ the slope of the normal compression line (NCL) in the space of the logarithmic mean stress $\ln p'$ versus the void ratio e
- κ the slope of the unloading–reloading line (URL) in the $\ln p'$–e space
- e_N the intercept of the NCL on the e-axis when $\ln p' = 0$
- ν the Poisson's ratio of the soil skeleton
- OCR the over-consolidation ratio of the soil
- K_o the coefficient of earth pressure at rest
- γ the unit weight of the soil, and
- k_{xx}, k_{yy} coefficients of permeability in x and y directions, respectively.

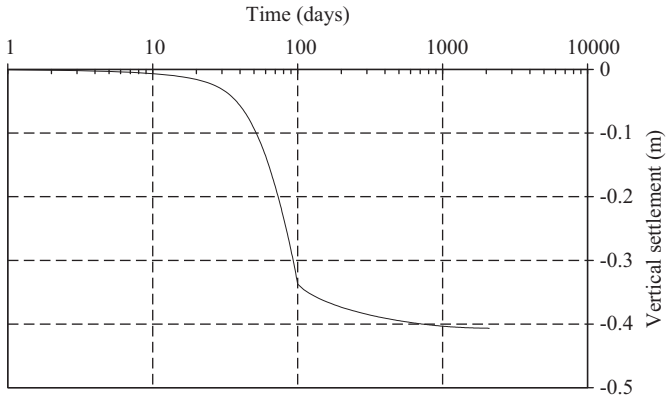

Fig. 7. Settlement versus time for the footing on MCC soil.

Because the MCC soil does not have any shear strength at zero mean stress, a thin layer of elastic material is added on top of the MCC soil to prevent a slope instability problem when the settlement of the footing becomes very large.

The analysis includes three stages. In the first stage, a non-zero initial stress field is generated by applying body force due to the self-weight of the soil. Then, the initial yield surface locations are determined according to the current stresses and the OCR. In the second stage, a uniform vertical pressure is applied to the footing at a constant rate over a period of 100 days until reaching a magnitude $q = 40$ kPa. Finally, the load q is then kept constant and the soil is allowed to consolidate over time.

Fig. 7 shows a plot of the settlement of the footing versus time obtained by the UL method. The final consolidation settlement of the footing is 0.41 m. All algorithms produced virtually identical results in this case. Note that neither severe mesh distortion nor entanglement of elements was observed in this example. This is shown graphically by plotting the deformed mesh at the end of the analysis in Fig. 8. Stress-integration time and total number of iterations are shown in Table 3 for each algorithm. According to the table, Algorithm 3 is 14% and 21% faster than Algorithms 1(a), (b) and 2(a), (b), respectively. It is also evident that Algorithm 3 requires fewer iterations to achieve equilibrium compared with Algorithms 1(a), (b) and 2(a), (b).

5. Conclusions

Three stress-integration algorithms for a rate-type large-deformation analysis were presented in this paper. In Algorithm 1, the stresses are corrected for rigid-body motion before integrating the stress–strain relations. Algorithm 2 integrates the constitutive equations and then corrects the stresses for possible rigid-body rotations. In Algorithm 3, the correction due to rigid-body rotation is introduced both in elastic and the elastoplastic stress increments during the stress integration. The following conclusions are drawn from the numerical examples considered in this paper:

(1) All three algorithms are capable of providing more or less identical results (provided load steps are sufficiently small), i.e., in terms of accuracy, there is no real advantage in choosing one algorithm over the others. This implies the stress correction due to rigid-body rotation may be calculated

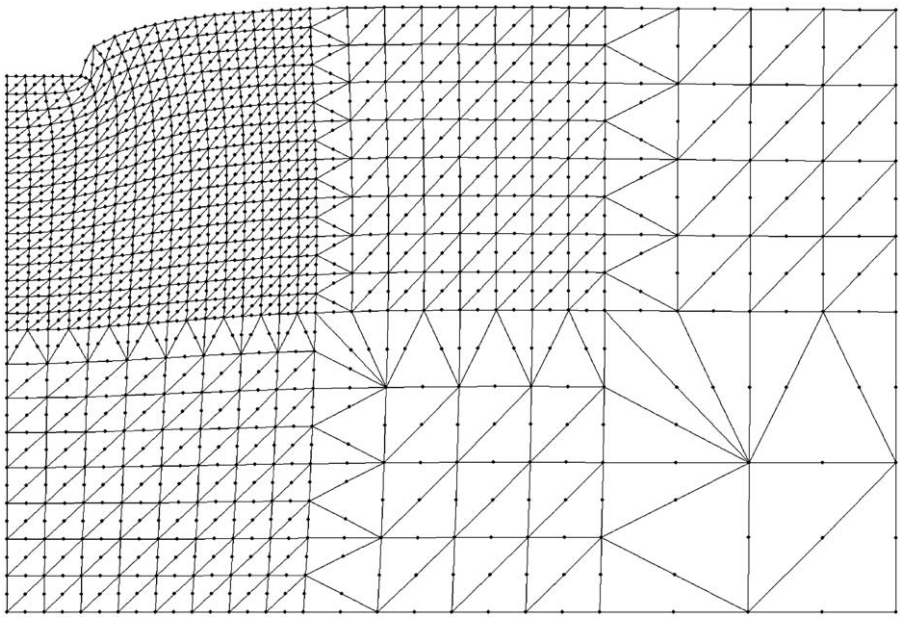

Fig. 8. Deformed mesh of the footing on MCC soil at the end of analysis.

Table 3
Stress-integration time and total iterations of alternative stress-integration algorithms—UL method.

Algorithm	Stress-integration time (s)	Total iterations
1	242	781
2	262	801
3	208	709

before, after, or during integration of the constitutive equations as long as an objective stress rate is employed.

(2) Any stress-integration algorithm developed for a small-deformation analysis can therefore be directly used in a large-deformation analysis without modification, provided that the stresses are corrected for rigid-body rotation by an auxiliary subroutine either before or after integrating the constitutive equations. This conclusion is very helpful in developing software for large-deformation analysis.

(3) Comparing the time spent for stress integration and the total number of iterations necessary to achieve equilibrium in each algorithm has revealed that it is slightly more efficient to apply rigid-body corrections while integrating the constitutive equations. This may be due to the fact that increments of strain and rigid-body motion are derived from the same displacement increments. Consequently, it is more reasonable to integrate the two increments simultaneously. This statement has been shown to be true for the examples presented here by the fact that Algorithm 3 is faster than Algorithms 1(a), (b) and 2(a), (b), requiring fewer iterations to achieve equilibrium during a load increment.

Finally, it is emphasised that these conclusions are based on a study of only two example problems, but both involved very severe straining of the elastoplastic medium and large displacements and rotations. On this basis it is speculated that these conclusions should apply much more broadly.

Acknowledgements

The research described in this paper was supported by Discovery Project grants funded by the Australian Research Council. This support is gratefully acknowledged.

References

[2] K.J. Bathe, E. Ramm, E.L. Wilson, Finite element formulations for large deformation dynamic analysis, International Journal for Numerical Methods in Engineering 9 (1975) 353–386.
[3] T. Belytschko, W.K. Liu, B. Moran, Nonlinear Finite Elements for Continua and Structures, John Wiley, Chichester–New York, 2000.
[4] J.P. Carter, J.R. Booker, E.H. Davis, Finite deformation of an elasto-plastic soil, International Journal for Numerical and Analytical Methods in Geomechanics 1 (1977) 25–43.
[5] J.P. Carter, J.C. Small, J.R. Booker, A theory of finite elastic consolidation, International Journal of Solids and Structures 13 (1977) 467–478.
[6] M.A. Crisfield, Nonlinear Finite Element Analysis of Solids and Structures, vol. 1, John Wiley and Sons, Chichester, England, 1991.
[7] M. Dowell, P. Jarratt, The Pegasus method for computing the root of an equation, BIT Numerical Mathematics 12 (1972) 503–508.
[8] M.S. Gadala, J. Wang, Computational implementation of stress integration in FE analysis of elasto-plastic large deformation problems, Finite Elements in Analysis and Design 35 (2000) 379–396.
[9] T.J.R. Hughes, J. Winget, Finite rotation effects in numerical integration of rate constitutive equations arising in large-deformation analysis, International Journal for Numerical Methods in Engineering 15 (1980) 1862–1867.
[10] M. Nazem, D. Sheng, J.P. Carter, Stress integration and mesh refinement in numerical solutions to large deformations in geomechanics, International Journal for Numerical Methods in Engineering 65 (2006) 1002–1027.
[11] M. Nazem, D. Sheng, J.P. Carter, S.W. Sloan, Arbitrary Lagrangian–Eulerian method for large deformation consolidation problems in geomechanics, International Journal for Analytical and Numerical Methods in Geomechanics 32 (2008) 1023–1050.
[12] P.M. Pinsky, M. Ortiza, K.L. Pister, Numerical integration of rate constitutive equations in finite deformation analysis, Computer Methods in Applied Mechanics and Engineering 40 (1983) 137–158.
[13] A. Rodriguez-Ferran, A. Huerta, Comparing two algorithms to add large strains to small-strain FE code, Journal of Engineering Mechanics 124 (1998) 939–948.

[14] S.W. Sloan, Substepping schemes for the numerical integration of elastoplastic stress–strain relations, International Journal for Numerical Methods in Engineering 24 (1987) 893–911.
[15] S.W. Sloan, A.J. Abbo, D. Sheng, Refined explicit integration of elastoplastic models with automatic error control, Engineering Computations 18 (2001) 121–154.
[16] S.W. Sloan, A.J. Abbo, D. Sheng, Erratum, Engineering Computations 19 (2002) 594.
[17] J. Zhao, D. Sheng, M. Rouainia, S.W. Sloan, Explicit stress integration of complex soil models, International Journal for Analytical and Numerical Methods in Geomechannics 29 (2005) 1209–1229.